

## Evidence for cluster spin glass phase with precursor short-range antiferromagnetic correlations in the $B$ -site disordered $\text{Ca}(\text{Fe}_{1/2}\text{Nb}_{1/2})\text{O}_3$ perovskite

Arun Kumar,<sup>1</sup> Anatoliy Senyshyn,<sup>2</sup> and Dhananjai Pandey<sup>1,\*</sup>

<sup>1</sup>*School of Materials Science and Technology, Indian Institute of Technology (Banaras Hindu University), Varanasi-221005, India*

<sup>2</sup>*Forschungszentrum für Neutronenphysik und Neutronenoptik, Technische Universität München, Lichtenbergstrasse 1, D-85747 Garching, Germany*



(Received 10 March 2019; published 18 June 2019)

The origin of the spin glass (SG) phase in the well-known multiferroic  $\text{Pb}(\text{Fe}_{1/2}\text{Nb}_{1/2})\text{O}_3$  compound remains controversial due to the complications introduced by the coexistence of SG and long-range ordered (LRO) antiferromagnetic (AFM) phases. We have addressed this controversy through a comprehensive study on a Pb-free system  $\text{Ca}(\text{Fe}_{1/2}\text{Nb}_{1/2})\text{O}_3$  (CFN) which does not exhibit LRO AFM transition. The SG transition in CFN is confirmed by the appearance of a cusp in the temperature dependence of dc magnetization  $M(T)$  with a SG freezing temperature  $T_f \sim 25$  K, and bifurcation of the zero-field-cooled and field-cooled magnetization  $M(T)$  below the irreversibility temperature  $T_{ir} \sim 27$  K. Using ac susceptibility [ $\chi(\omega, T)$ ] measurements, we show that the spin dynamics follows power/Vogel-Fulcher law-type critical dynamics which diverges at  $T_{SG} \sim 24$  K with an attempt time  $\tau_0 \sim 10^{-6}$  s suggesting cluster spin glass (CSG) behavior. The field dependence of  $T_f(H)$  and  $T_{ir}(H)$  is shown to follow the de Almeida–Thouless line which separates the ergodic and nonergodic phases in the  $H$ - $T$  plane and gives  $T_f(H=0) \sim 25$  K, which is in close agreement with  $T_{SG}$  obtained from  $\chi(\omega, T)$ . The existence of the glassy phase below  $T_{SG}$  is further confirmed by the observation of slow nonexponential decay of thermoremanent magnetization with time, memory and rejuvenation effects, and unidirectional exchange-bias effect in the  $M$ - $H$  hysteresis loop of field-cooled samples. The neutron powder-diffraction patterns reveal the absence of any magnetic peak due to LRO AFM phase but show a broad diffuse peak due to the presence of  $\sim 2$ -nm-size AFM spin clusters which are responsible for the CSG freezing in CFN.

DOI: [10.1103/PhysRevB.99.214425](https://doi.org/10.1103/PhysRevB.99.214425)

### I. INTRODUCTION

Complex perovskites with a general formula of the type  $(A' A'')(B' B'')\text{O}_3$ , where the  $A/B$ -site cations may be ordered or disordered depending upon the difference in their ionic radii and valence, are known for their wide-ranging functional properties [1–8]. One of the unique features of such complex perovskites is that the ratio of  $A' : A''$  or  $B' : B''$  is fixed like 1 : 1, 1 : 2, and 1 : 3, akin to compounds obeying normal valence rules but unlike the solid-solution systems. However, the nature of their occupancy at the  $A$  or  $B$  site of  $\text{ABO}_3$  perovskite lattice varies all the way from nearly ordered [9] to nearly disordered [10] depending on the compounds, and sometimes in the same compound also as a result of long-term annealing [10]. Within the broad family of such site- and charge-disordered/ordered compounds, complex perovskites with the formula  $A(B'_{1/2}B''_{1/2})\text{O}_3$ , where  $B' : B''$  are in 1 : 1 ratio, commonly known as double perovskites, have received immense attention from the point of view of the colossal magnetoresistance [11–13], half metallicity [14–16], metal to insulator transition [17–19], superconductivity [20,21], etc.), normal ferroelectricity [9] and relaxor ferroelectricity [4–6,22–24], long-range magnetic ordering [25–31], and multiferroicity [32–35]. Multiferroicity in the double perovskites of the type  $A(B'_{1/2}B''_{1/2})\text{O}_3$  with  $A = \text{Pb}, \text{Ba}, \text{Sr}, \text{Ca}$  can be

easily introduced by choosing one of the  $B$ -site cations with partially filled  $d$  orbitals ( $d^n$ ) imparting magnetic properties (e.g., Cr, Mn, Fe, Co, Ni, Ru, Re, Os, Ir) and the other with unfilled  $d$  orbitals ( $d^0$ ) (e.g., Nb, Sb, Ta, W, Mo) required for inducing ferroelectric distortion [36], as was first demonstrated by Russian scientists who synthesized these complex multiferroic perovskites nearly six decades back [37–39].

Among the complex double perovskites with  $B$ -site disorder, the niobate family has evinced considerable interest and  $\text{Pb}(\text{Fe}_{1/2}\text{Nb}_{1/2})\text{O}_3$  (PFN) has emerged as a model type-I multiferroic niobate system [30,31,37–46]. It undergoes a paraelectric (space group  $Pm-3m$ ) to ferroelectric (space group  $Cm$ ) transition at  $T_c \sim 385$  K [43,44],  $G$ -type long-range ordered (LRO) antiferromagnetic (AFM) phase below  $T_N \sim 150$  K [45,46], and a spin glass (SG) freezing at  $T_f \sim 10$  K [30,31]. It has been proposed that LRO is of percolative type in which all the six nearest-neighbor superexchange  $\text{Fe}^{3+}-\text{O}^{2-}-\text{Fe}^{3+}$  bonds are not necessarily satisfied everywhere (unless there is clustering and segregation of Fe) [30]. Interestingly, this LRO AFM phase is found to coexist with the SG phase below  $T_f \sim 10$  K but there is a controversy about the exact origin of the coexistence of the two phases [30,31,46]. According to one of these models based on macroscopic measurements, the LRO AFM phase of PFN results from the infinite percolative clusters of  $\text{Fe}^{3+}$  spins while the glassy phase is a consequence of the freezing of the finite-size isolated clusters with uncompensated  $\text{Fe}^{3+}$  spin [30]. This model implies that the SG and LRO AFM phases occur on

\*dp.mst1979@gmail.com

two separate sublattices. However, no direct evidence for the presence of such nanoscale heterogeneities was presented in Ref. [30] as it requires microscopic probes like neutron scattering and Mössbauer studies [31,46]. In the second model, which is supported by microscopic measurements (neutron and Mössbauer techniques), on the other hand, the SG phase is argued to result from the LRO AFM sublattice system itself due to freezing of the transverse component of the spin in a glassy manner [31]. It is worth mentioning here that the study of SG transition in ordered [29,47–49] and disordered [29,50–52] double perovskites continues to attract enormous attention in the current literature.

Unlike PFN, the Pb-free site- and charge-disordered  $A(\text{Fe}_{1/2}B'_{1/2})\text{O}_3$ -type compounds with  $A = \text{Ba}, \text{Sr}, \text{Ca}$  and  $B' = \text{Nb}$  and  $\text{Ta}$  do not display LRO ferroelectric and AFM phases, despite  $\text{Nb}^{5+}$  being a ferroactive ion of  $4d^0$  type [36] and the concentration of  $3d \text{Fe}^{3+}$  moments at the  $B$  site being higher than the typical percolation threshold [53], respectively. This difference has been attributed to the absence of  $6s^2 \text{Pb}^{2+}$  lone-pair chemistry in the Pb-free compounds [54]. The Pb-free complex perovskite niobates and tantalates are also reported to exhibit SG freezing at low temperatures with  $T_f \sim 25 \text{ K}$  [55–58] like PFN [30,31]. Since the controversy about the origin of the SG phase in PFN is essentially due to the coexistence of the LRO and the SG phases, the Pb-free complex perovskite niobates and tantalates with no such coexistence offer an excellent platform to verify the origin of SG phase due to nanoscale antiferromagnetically correlated spin clusters proposed in Ref. [30]. With this objective in mind, we present here the results of a comprehensive study on  $\text{Ca}(\text{Fe}_{1/2}\text{Nb}_{1/2})\text{O}_3$  (CFN) using both macroscopic and microscopic measurements. The previous reports of SG state in Pb-free complex perovskite niobates and tantalates, including CFN, are based on the observation of the history-dependent irreversibility of zero-field-cooled (ZFC) and field-cooled (FC) dc magnetization  $M(T)$  plots only [55–58], which is not conclusive as such an irreversibility can also occur due to superparamagnetic (SPM) blocking [59]. Further, unlike PFN, there is no neutron-scattering study which could have provided direct evidence for the presence of short-range ordered (SRO) AFM spin clusters in such compounds. We have used multiple criteria [60,61] based on dc magnetization [ $M(T)$ ,  $M(H)$ ,  $M(t)$ ] and ac susceptibility [ $\chi(\omega, T)$ ]

measurements for confirming the existence of the SG phase in CFN. In addition, we use neutron-scattering measurements to confirm the presence of SRO AFM spin clusters in CFN.

## II. EXPERIMENTAL

### A. Sample preparation

Polycrystalline sample of CFN was synthesized by standard solid-state route using high-purity carbonate ( $\text{CaCO}_3$ ) and oxides ( $\text{Fe}_2\text{O}_3$ ,  $\text{Nb}_2\text{O}_5$ ) supplied by Sigma-Aldrich. The stoichiometric powders were first mixed with an agate mortar and pestle for 2 h. The mixture was then ball milled (Retsch GmbH, Germany) for 6 h with acetone as mixing media using zirconia jar and zirconia balls. After evaporation of the acetone, the mixed powder was calcined at 1423 K for 10 h in an open alumina crucible. The calcined powder was crushed into fine powder and again ball milled for 4 h, dried, and then pressed into pellets at an optimized load of 70 kN using 2% polyvinyl alcohol solution as a binder. After binder burn-off at 773 K for 10 h, sintering was carried out at 1523 K for 3 h in open air. Powders obtained after crushing the sintered pellets were annealed at 773 K for 10 h to remove any strains developed during crushing. The annealed powders were used in all the measurements.

### B. Characterizations

The room-temperature high-resolution synchrotron x-ray powder diffraction (SXRD) data were collected at P02.1 beamline of PETRA III, Hamburg, Germany, at a wavelength of  $0.2079 \text{ \AA}$  ( $\sim 60 \text{ keV}$ ). Neutron powder-diffraction (NPD) data were collected using high-resolution powder diffractometer SPODI at FRM II Germany, at a wavelength of  $1.5482 \text{ \AA}$ . The structure was refined by Rietveld technique using software package FULLPROF [62]. Microstructure and chemical compositions of the  $\text{Ca}(\text{Fe}_{1/2}\text{Nb}_{1/2})\text{O}_3$  sample were checked by using a Carl-Zeiss scanning electron microscope (SEM), model no. EVO 18. The chemical compositions were also checked by electron probe microanalyzer (EPMA) using a CAMECA SXFive instrument. The dc and ac magnetization measurements were carried out on a superconducting quantum interference device-based magnetometer (Quantum Design, MPMS-3).

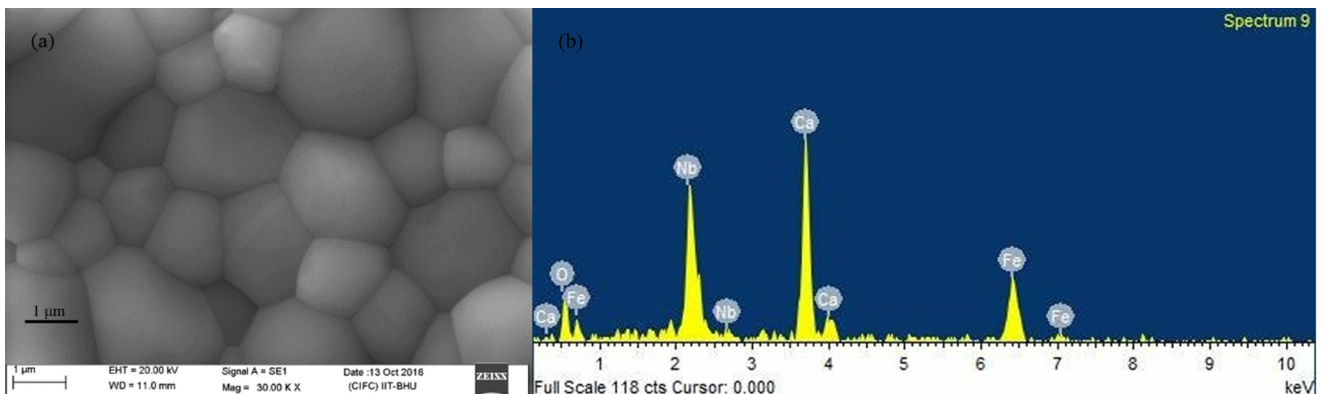


FIG. 1. Scanning electron micrograph and EDX spectra of  $\text{Ca}(\text{Fe}_{1/2}\text{Nb}_{1/2})\text{O}_3$ .

TABLE I. Quantification of  $\text{Ca}(\text{Fe}_{1/2}\text{Nb}_{1/2})\text{O}_3$  by EDX and EPMA analysis.

Average chemical composition in wt %				
Element	Expected	Observed by		
		EDX	EPMA	
Ca	24.7	$24.1 \pm 1.0$	$23.8 \pm 0.5$	
Fe	17	$17.3 \pm 1.0$	$16.7 \pm 0.2$	
Nb	28.6	$29.8 \pm 0.5$	$28.9 \pm 0.8$	
O	30	$28.7 \pm 0.8$	$28.3 \pm 0.5$	

### III. RESULTS AND DISCUSSION

#### A. Microstructure, chemical composition, phase purity, and crystal structure

The SEM image of the microstructure of CFN is shown in Fig. 1(a). The average grain size calculated by linear intercept method is found to be approximately  $1.4 \mu\text{m}$ . The Energy-dispersive X-ray spectra (EDX) of CFN are shown in the right panel [see Fig. 1(b)] and the chemical composition of the sample was determined through a quantitative analysis of the EDX spectra. The average composition of the ceramic sample was confirmed through EPMA analysis also as its results are more accurate. The results of EDX and EPMA are compared in Table I, which confirms that the composition of the samples corresponds to the nominal composition within the standard deviation. The absence of any impurity phase in the SXRD pattern of CFN confirms that the CFN powders are monophasic. Its orthorhombic crystal structure in the  $Pbnm$  space group [56,63,64] was verified using Rietveld refinement technique. The asymmetric unit of the orthorhombic phase of CFN consists of  $\text{Ca}^{2+}$ ,  $\text{Fe}^{3+}/\text{Nb}^{5+}$ ,  $\text{O}^{2-}_{\text{I}}$ , and  $\text{O}^{2-}_{\text{II}}$ , at  $(x, y, 1/4)$ ,  $(1/2, 0, 0)$ ,  $(x, y, 1/4)$ , and  $(x, y, z)$  corresponding to the Wyckoff sites  $4c$ ,  $4b$ ,  $4c$ , and  $8d$ , respectively. In the refinement, the background and peak shape were modeled with linear interpolation and pseudo-Voigt function, respectively while the occupancy was fixed at the nominal composition. Zero correction, scale factor, background, lattice parameters, half-width parameters ( $u, v, w$ ), positional coordinates, and thermal parameters were varied during the refinement which converged after a few cycles with the agreement factor  $R_{\text{wp}} = 1.37\%$  and  $\chi^2 = 1.15$ . Figure 2(a) depicts the observed (filled circles) and calculated (continuous line) profiles which are in excellent agreement as can be seen from the difference profile (bottom line) in the same figure. The Rietveld refinement using SXRD data

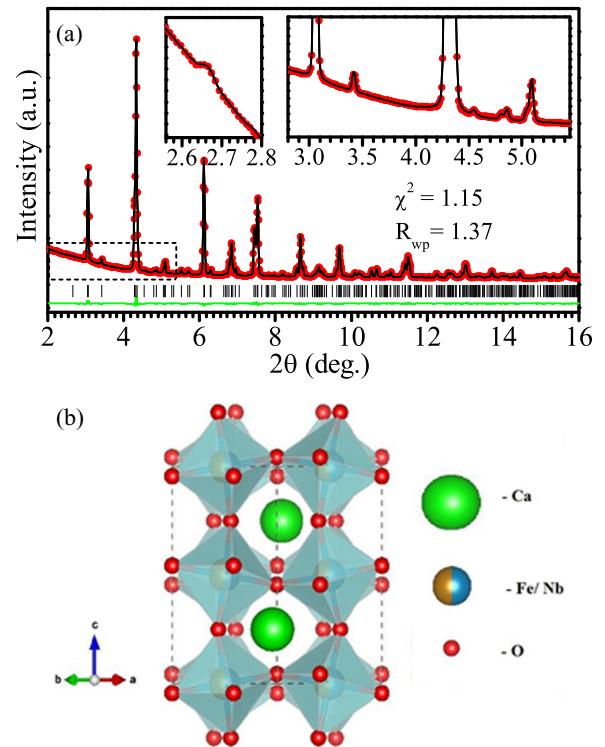


FIG. 2. (a) Observed (red dots), calculated (black continuous line), and difference (green continuous line) profiles obtained from Rietveld refinement of synchrotron x-ray pattern of  $\text{Ca}(\text{Fe}_{1/2}\text{Nb}_{1/2})\text{O}_3$  at room temperature using  $Pbnm$  space group. Vertical tick marks above the difference profile represent the Bragg peak positions. The insets show the superlattice peaks fit on an enlarged scale; (b) depicts the crystal structure of  $\text{Ca}(\text{Fe}_{1/2}\text{Nb}_{1/2})\text{O}_3$  along with tilted octahedra.

thus confirms that CFN belongs to orthorhombic phase in the  $Pbnm$  space group in agreement with the previous reports [56,63,64]. The orthorhombic structure of CFN belongs to the  $a^-a^-c^+$  tilt system in Glazer's notation [65]. The alternative space group  $P2_1/n$  proposed in some papers [64,66,67] considering oxygen octahedral tilts as well as 1:1 ordering of  $\text{Fe}^{3+}$  and  $\text{Nb}^{5+}$  ions can be rejected as it requires the presence of a superlattice peak around  $2\theta \sim 2.63^\circ$ ,  $3.75^\circ$ , and  $4.62^\circ$ , which is not seen in the SXRD pattern [68] as shown in Fig. S1 of the Supplemental Material. The refined structural parameters given in Table II are in good agreement with the values reported in the literature [56,63,64]. Figure 2(b) depicts the orthorhombic crystal structure of CFN along with the tilted oxygen octahedra.

TABLE II. Rietveld refined structural parameters of  $\text{Ca}(\text{Fe}_{1/2}\text{Nb}_{1/2})\text{O}_3$ .

Ions	$x$	$y$	$z$	$B$ ( $\text{\AA}^2$ )
$\text{Ca}^{2+}$	0.0083(5)	0.0439(2)	1/4	1.01(2)
$\text{Fe}^{3+}/\text{Nb}^{5+}$	1/2	0	0	0.28(9)
$\text{O}^{2-}_{\text{I}}$	0.2953(5)	0.2916(4)	0.0425(4)	0.77(5)
$\text{O}^{2-}_{\text{II}}$	0.9170(7)	0.4771(6)	1/4	1.02(7)

$A_0 = 5.4480(1) \text{\AA}$ ,  $B_0 = 5.5499(1) \text{\AA}$ ,  $C_0 = 7.7573(2) \text{\AA}$  :  $\alpha = \beta = \gamma = 90^\circ$

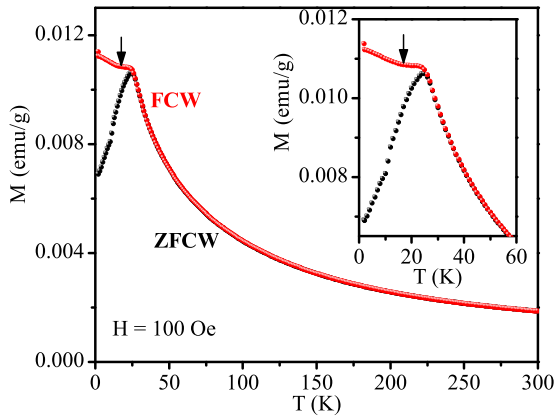


FIG. 3. Temperature dependence of dc magnetization of  $\text{Ca}(\text{Fe}_{1/2}\text{Nb}_{1/2})\text{O}_3$  measured at 100 Oe field in warming cycle for both ZFC and FC conditions. The inset gives a magnified view of the  $M(T)$  to reveal a small dip (marked with an arrow) in the FCW  $M(T)$  below  $T_f$ .

### B. Evidence for history-dependent irreversibility: dc magnetization studies

The temperature dependence of dc magnetization  $M(T)$  of CFN measured during warming under a magnetic field of 100 Oe after ZFC of the sample (we shall call this protocol ZFCW henceforth) shows a peak at  $T_f \sim 25$  K in agreement with previous reports on CFN [56]. The disordered complex perovskites like  $\text{Sr}(\text{Fe}_{1/2}\text{Nb}_{1/2})\text{O}_3$  (SFN),  $\text{Ba}(\text{Fe}_{1/2}\text{Nb}_{1/2})\text{O}_3$  (BFN),  $\text{Ca}(\text{Fe}_{1/2}\text{Ta}_{1/2})\text{O}_3$  (CFT),  $\text{Sr}(\text{Fe}_{1/2}\text{Ta}_{1/2})\text{O}_3$  (SFT), and  $\text{Ba}(\text{Fe}_{1/2}\text{Ta}_{1/2})\text{O}_3$  (BFT) also show  $T_f$  around 25 K [56–58]. Pb-based disordered complex perovskites, like PFN,  $\text{Pb}(\text{Fe}_{1/2}\text{Ta}_{1/2})\text{O}_3$  (PFT),  $\text{Pb}(\text{Fe}_{2/3}\text{W}_{1/3})\text{O}_3$ , on the other hand, show lower  $T_f \sim 10$  K [30,31,69–71].

Curie-Weiss (CW) fit to the ZFCW  $M(T)$  above 240 K yields Curie constant  $C = 1.138 \text{ emu K mol}^{-1} \text{ Oe}^{-1}$  and CW temperature  $\theta_w = -76.8$  K. The effective magnetic moment ( $\mu_{\text{eff}}$ ) obtained from the Curie constant after taking into account 50% dilution of the magnetic sublattice due to  $\text{Nb}^{5+}$  substitution comes out to be  $3.02 \mu_B$ , which is in close agreement with the previous reports on SFN, BFN, CFT, SFT, and BFT also [56–58]. The large negative value of Curie-Weiss temperature reveals predominant antiferromagnetic exchange interactions in CFN but there is no signature of any AFM transition in the ZFCW  $M(T)$  plot of CFN in marked contrast to PFN and PFT, which show a small anomaly at  $T_N \sim 150$  K [30,31,69,70].

The ZFCW and FCW  $M(T)$  plots at 100 Oe field shown in Fig. 3 reveal bifurcation of the two curves, at the irreversibility temperature  $T_{\text{irr}} \sim 27$  K, which is a characteristic of SG freezing [60,61]. However, such a bifurcation is known to occur in an ensemble of noninteracting SPM spin clusters due to the onset of blocking dynamics at  $T_{\text{irr}}$  [59]. The FCW  $M(T)$  curve for noninteracting SPM systems is known to increase continuously below  $T_B$ , whereas in our case the FCW  $M(T)$  curve is nearly flat just below  $T_f/T_B$  over a narrow temperature range before it begins to rise again. Such a behavior is known to occur in cluster spin glass (CSG) systems with interacting spin clusters [59].

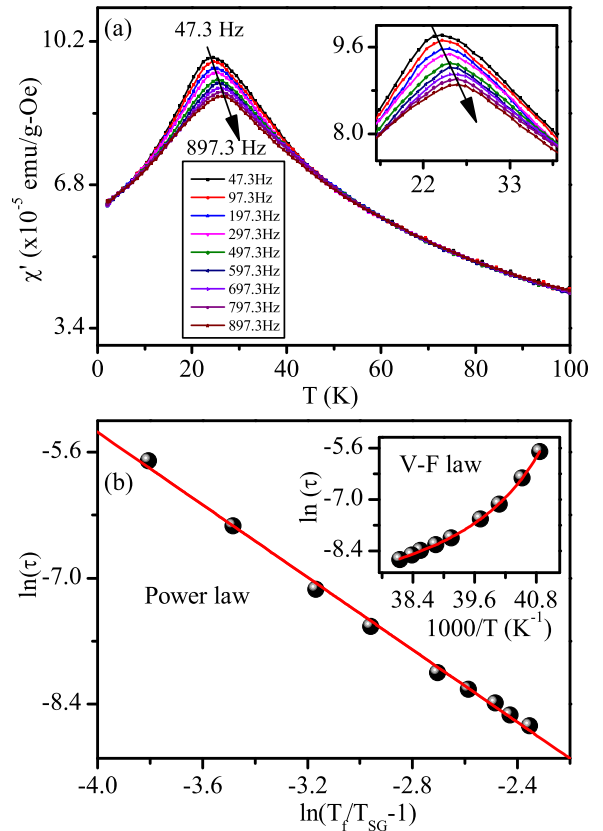


FIG. 4. (a) Temperature dependence of the real part  $[\chi'(\omega, T)]$  of ac magnetic susceptibility of  $\text{Ca}(\text{Fe}_{1/2}\text{Nb}_{1/2})\text{O}_3$  measured at various frequencies as labeled in the plot for an applied ac drive field of 1 Oe. The main panel (b) depicts  $\ln(\tau)$  versus  $\ln(T_f/T_{\text{SG}} - 1)$  plot, where  $\tau = 1/(2\pi f)$ . Inset to panel (b) depicts the  $\ln(\tau)$  versus  $1/T$  plot. The solid line represents the least-squares fit for critical power law and Vogel-Fulcher law.

### C. Evidence for critical slowing down of the spin dynamics: ac susceptibility studies

The analysis of the dc magnetization data presented in the previous section indicates the existence of SG freezing with  $T_f \sim 25$  K. In order to rule out the possibility of SPM blocking leading to the peak in ZFCW dc  $M(T)$  and bifurcation of ZFCW and FCW  $M(T)$ , we carried out a study of the spin/cluster dynamics using frequency- and temperature-dependent ac magnetic susceptibility  $[\chi(\omega, T)]$  measurements. Figure 4(a) depicts the variation of the real  $[\chi'(\omega, T)]$  part of ac susceptibility of CFN measured at various frequencies for an applied ac drive field of 1 Oe. It is evident from the figure that the temperature corresponding to the peak in the  $\chi'(\omega, T)$  plot shifts to higher temperatures side with increasing frequency. Although a frequency-dependent shift of  $T_f(\omega)$  is known for both SG freezing and SPM blocking [59–61], a distinction between the two can be made using the empirical Mydosh parameter ( $K$ ) defined as [60]

$$K = \frac{1}{T_f(\omega)} \frac{\Delta T_f(\omega)}{\Delta(\ln \omega)}, \quad (1)$$

where  $\Delta T_f(\omega)$  is the difference between the peak temperatures of  $\chi'(\omega, T)$  at low and high frequencies. For SG/CSG

freezing, the Mydosh parameter lies in the range 0.005–0.09 whereas it usually lies in the 0.1–0.3 range for SPM blocking [60,61,72]. In the present case, the Mydosh parameter comes out to be 0.045 which suggests that the frequency dispersion of  $T_f(\omega)$  is due to SG/CSG freezing and not SPM blocking.

The frequency dependence of the SG freezing temperature  $[T_f(\omega)]$  in the scaling theories of spin glasses has been modeled using a power-law behavior which predicts critical slowing down of the spin dynamics and its divergence at  $T_{SG}$  at which the ergodic symmetry is broken [73]:

$$\tau = \tau_0 \left( \frac{T_f(\omega) - T_{SG}}{T_{SG}} \right)^{-z\nu}, \quad (2)$$

where  $\tau_0$  is the inverse of the attempt frequency (i.e., attempt time),  $T_{SG}$  the SG transition temperature at which  $\tau$  diverges,  $\nu$  the critical exponent of the correlation length  $\xi = (T_f/T_{SG} - 1)^{-\nu}$  and  $z$  the dynamic exponent  $\tau \sim \xi^z$ . The relaxation time  $\tau$  corresponding to the peak temperature  $T_f(\omega)$  for each measuring frequency  $\omega = 2\pi f$  was determined using  $\tau = 1/2\pi f$ . A least-square fit to the  $\ln(\tau)$  versus  $\ln(T_f/T_{SG} - 1)$  plot shown with solid line in Fig. 4(b) gives  $T_{SG} = (23.9 \pm 0.4)$  K,  $\tau_0 = 1.47 \times 10^{-6}$  s, and  $z\nu = (2.01 \pm 0.04)$ . The large value of  $\tau_0$  reveals slow dynamics as expected for cluster spin glasses for which  $\tau_0$  typically lies in the range  $\sim 10^{-6}$ – $10^{-10}$  s [60,61]. Such high  $\tau_0$  values have been reported in several CSG systems [74–76]. For canonical SG systems like Cu:Mn, the value of  $\tau_0$  is of the order of  $\sim 10^{-13}$  s, which is several orders of magnitude smaller than that for the cluster spin glasses [60,61].

In order to cross-check the CSG dynamics, we modeled  $T_f(\omega)$  using the Vogel-Fulcher (VF) law also which has been used to describe the critical spin dynamics in some spin glasses [77]:

$$\tau = \tau_0 \exp \left( \frac{E_a}{k_B [T_f(\omega) - T_{VF}]} \right), \quad (3)$$

where  $E_a$  is the activation energy,  $k_B$  the Boltzmann constant, and  $T_{VF}$  [which is equivalent to  $T_{SG}$  in Eq. (2)] is called Vogel-Fulcher freezing temperature at which the spin dynamics diverges. SPM blocking dynamics, unlike the SG critical dynamics, does not show critical slowing down of the relaxation time but exhibits Arrhenius type of noncritical behavior with  $T_{VF} = 0$  in Eq. (3). The  $\ln(\tau)$  vs  $(1/T)$  plot for Arrhenius dynamics should obviously be linear. The nonlinearity of this plot shown in the inset of Fig. 4(b) clearly rules out SPM blocking process to be responsible for the peak in the ZFCW dc magnetization or ac susceptibility. On the other hand, VF law provides an excellent fit as shown with a continuous line through the data points in the inset. The least-squares fitting parameters for VF law are  $T_{VF} = (23.3 \pm 0.1)$  K,  $E_a = 0.495$  meV, and  $\tau_0 = 2.51 \times 10^{-6}$  s. The  $T_{SG}$  and  $\tau_0$  obtained using power law are comparable to  $T_{VF}$  and  $\tau_0$  for the VF law. It is worth mentioning here that the value of activation energy  $E_a = 0.495$  meV (i.e., 5.74 K) is comparable to the activation energies reported for frustrated CSG systems (e.g.,  $\text{Eu}_x\text{Sr}_{1-x}\text{S}$ ) but lower than those for the canonical Ruderman-Kittel-Kasuya-Yosida-type spin glasses [77]. Thus, both the power-law and Vogel-Fulcher fits confirm CSG freezing in CFN with  $T_{SG} \sim 24 \pm 1$  K.

#### D. Evidence for the existence of de Almeida–Thouless line in the $H$ - $T$ plane

Using the concept of replica symmetry breaking [78], it has been shown theoretically that the irreversibility temperature  $T_{irr}$ , which nearly coincides with  $T_f$  for canonical SG systems [60], would shift towards lower temperatures in the presence of magnetic field for both the Ising and Heisenberg systems [60,61]. The field dependence of  $T_{irr}/T_f$  [i.e.,  $T_{irr}(H)/T_f(H)$ ] is predicted to follow the following relationship at low fields:

$$H(T) \propto \left( 1 - \frac{T_f(H)}{T_f(0)} \right)^m, \quad (4)$$

where the characteristic exponent  $m$  takes the value 3/2 or 1/2 for de Almeida–Thouless (AT) [79] or Gabay-Toulouse lines [80–82] in the  $H$ - $T$  plane. To verify the stability of the SG phase of CFN in the presence of magnetic field, we depict the ZFCW and FCW  $M(T)$  plots of CFN at various fields in Fig. 5. It is evident from the figure that the irreversibility temperature  $T_{irr}$ , marked with an arrow pointing downwards, shifts to the lower temperature side on increasing the magnetic field in agreement with the theoretical predictions [79–82]. Further, the SG freezing temperature  $T_f(H)$ , shown with an arrow pointing upwards in the same figure, corresponding to the peak in the ZFCW  $M(T)$  also decreases with increasing magnetic field. Figure 6 depicts a plot of  $T_{irr}$  versus  $H^{2/3}$  as well as  $T_f(H)$  versus  $H^{2/3}$ . It can be seen from this figure that both the plots are linear below 7500 Oe, confirming AT-type field dependence of  $T_{irr}(H)$  as well as  $T_f(H)$ . The extrapolation of the AT line to  $H = 0$  gives the SG transition temperature  $T_{SG} \sim 27.1$  and 25.2 K, using  $T_{irr}(H)$  and  $T_f(H)$  temperatures, respectively. The difference between  $T_{irr}(H)$  and  $T_f(H)$  at each field is about 2 K, which is also reflected in the  $T_{SG}$  temperature obtained from these two characteristic temperatures. We note that the value of  $T_{SG} \sim 25.2$  K obtained from  $T_f(H)$  versus  $H^{2/3}$  plot is closer to that obtained from power-law/Vogel-Fulcher spin dynamics.

The AT line has been reported for both the canonical SG as well as CSG systems using field dependence of either  $T_{irr}(H)$  [83–85] or  $T_f(H)$  [30,86–89] and represents the boundary between the high-temperature ergodic and low-temperature nonergodic phases. While the original formulation for the AT line was for Ising spins [79], subsequent theoretical papers have shown that it can occur in Heisenberg systems also if the single-ion anisotropy is low and positive [82]. It is therefore not possible to comment on the nature of the spins (Ising versus Heisenberg) in CFN on the basis of Fig. 6.

#### E. Other characteristic features of the spin glass phase of CFN

Having confirmed the existence of CSG freezing with  $T_f \sim 25$  K in CFN using multiple criteria, we now proceed to examine the three characteristic properties of glassy state, namely slow relaxation of the thermoremanent magnetization [60,61,90], memory and rejuvenation effects [59], and unidirectional exchange-bias effects [60,61]. The slow relaxation of thermoremanent magnetization (TRM) below  $T_{SG}$  in SG and CSG systems has been a subject matter of theoretical and experimental investigations by several workers [30,83,90]. Palmer *et al.* [90] have presented a generalized theory for strongly interacting SG systems, including spin clusters, in

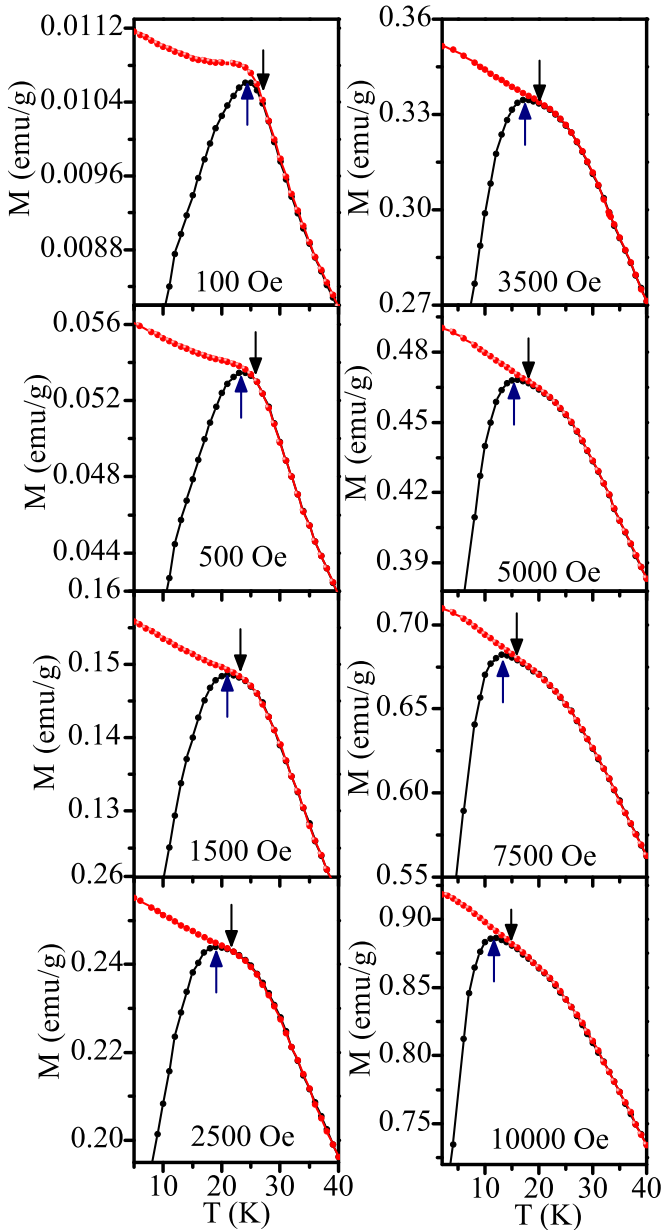


FIG. 5. Temperature dependence of the ZFCW and FCW dc magnetization plots of  $\text{Ca}(\text{Fe}_{1/2}\text{Nb}_{1/2})\text{O}_3$  at various applied magnetic fields.

terms of a hierarchically constrained dynamics and have shown that the time dependence of TRM should exhibit a stretched exponential behavior:

$$M(t) = M_0 \exp[-(t/\tau)^\beta], \quad (5)$$

where  $M_0$  is the initial magnetization at  $t = 0$ ,  $\tau$  the characteristic relaxation time, and  $\beta$  the exponent for the stretched exponential function. The value of  $\beta$  usually lies between 0 and 1 for different class of SG systems [59–61]. In this context,  $\beta = 1$  means the system has monodispersive Debye-like relaxation while  $\beta = 0$  implies absence of any relaxation. The intermediate values of  $\beta$  in the range  $0 < \beta < 1$  imply a non-Debye behavior with distribution of relaxation times due to the presence of a large number of degenerate states in the

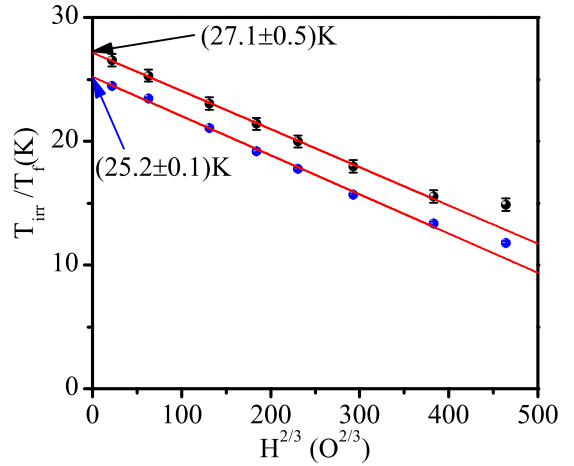


FIG. 6. Plot of  $T_{\text{irr}}$  versus  $H^{2/3}$  as well as  $T_f$  versus  $H^{2/3}$  showing the presence of de Almeida–Thouless line.

frozen state. We investigated the slow relaxation of the TRM in the glassy phase of CFN using the stretched exponential function given by Eq. (5). For this, the sample was first cooled in an applied magnetic field of 1000 Oe from 300 to 15 K (i.e., below the SG freezing temperature  $T_f$ ) and then allowed to age for a wait time  $t_w = 10^3$  s with field applied. After the waiting time, the field was switched off to zero and magnetization was measured as a function of time for  $10^4$  s. The results are shown in Fig. 7 where the continuous line shows the best fit to the stretched exponential function of Eq. (5) with  $M_0 = 0.035$ ,  $\tau = (40\,166 \pm 77)$  s, and  $\beta = 0.10$ . The value of the exponent  $\beta = 0.10$  not only lies in the typical range for spin glasses and cluster spin glasses but also indicates strongly polydisperse non-Debye relaxation, characteristic of the strongly interacting glassy systems in general [30].

Both spin glasses and cluster spin glasses are known to exhibit aging, memory and rejuvenation effects [59,83,91,92] due to chaotic ground state of the SG phase [93]. We followed two different protocols to verify the aging, memory and rejuvenation effects in the CSG phase of CFN. In the first protocol, the sample was initially cooled under zero field from  $T = 300$  K which is greater than  $T_f$  to a wait temperature

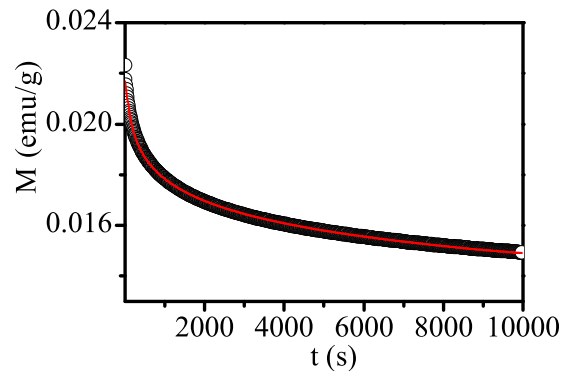


FIG. 7. Time dependence of thermoremanent magnetization of  $\text{Ca}(\text{Fe}_{1/2}\text{Nb}_{1/2})\text{O}_3$  sample at 15 K for 1000 Oe cooling field and wait time of 1000 s. The solid line is the best fit for stretched exponential function to the data.

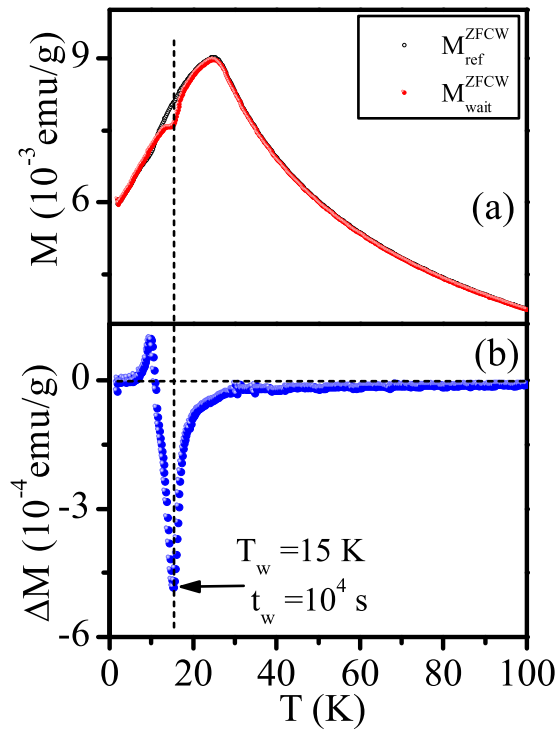


FIG. 8. (a) Temperature dependence of ZFC magnetization of  $\text{Ca}(\text{Fe}_{1/2}\text{Nb}_{1/2})\text{O}_3$  recorded at 100 Oe field with (•) and without (o) intermediate stop at  $T_w = 15$  K for a wait time ( $t_w$ ) of  $10^4$  s. (b) Depiction of the difference  $\Delta M(T) = M_{\text{wait}}^{\text{ZFCW}}(T) - M_{\text{ref}}^{\text{ZFCW}}(T)$  vs temperature ( $T$ ) plot from which it is evident that a sharp dip occurs exactly at the waiting temperature ( $T_w$ ).

$T_w = 15$  K, which is less than  $T_f \sim 25$  K, at which the sample was allowed to age for a wait time of  $t_w = 10^4$  s. After ageing for  $t = t_w$ , the sample was allowed to cool further in zero field down to 2 K. After such a zero-field cooling with an intermediate wait at  $T_w = 15$  K for  $t_w = 10^4$  s, the magnetization [ $M_{\text{wait}}^{\text{ZFCW}}(T)$ ] was measured during the heating cycle under 100 Oe field [see Fig. 8(a)]. This magnetization curve [ $M_{\text{wait}}^{\text{ZFCW}}(T)$ ] was compared with a reference curve  $M_{\text{ref}}^{\text{ZFCW}}(T)$  which was obtained by measuring magnetization during heating cycle under identical field (i.e., 100 Oe) after the sample was cooled in zero field up to 2 K without any intermediate stop at 15 K. Figure 8(b) depicts the difference  $\Delta M(T) = M_{\text{wait}}^{\text{ZFCW}}(T) - M_{\text{ref}}^{\text{ZFCW}}(T)$  vs temperature ( $T$ ) plot from which it is evident that a sharp dip occurs exactly at the waiting temperature ( $T_w$ ). Such a “hole burning” in the difference plot clearly demonstrates memory and rejuvenation effect in the CSG phase of CFN [59]. In the second protocol involving the FC condition [92], the sample was first cooled in 100 Oe magnetic field from 300 to 2 K at a constant rate of 2 K/min and then heated back continuously at the same rate and magnetization  $M(T)$  was recorded under the same field. This gives the reference curve [ $M_{\text{ref}}^{\text{FCW}}(T)$ ] shown with a continuous line in Fig. 9. This sample was cooled again from 300 to 2 K at the same rate of cooling (2 K/min) and under identical field (i.e., 100 Oe) but the sample was allowed to wait at two intermediate temperatures  $T = 50$  and 15 K, which are above and below  $T_f$ , respectively, for a wait time  $t_w = 3$  h each. The field was set to zero during the wait time at

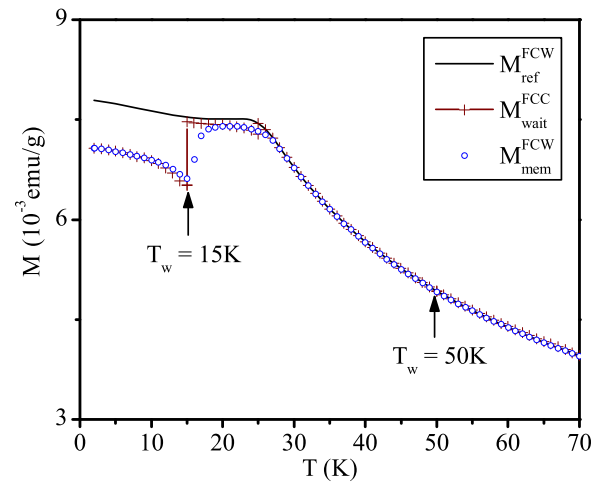


FIG. 9. Temperature dependence of dc magnetization of  $\text{Ca}(\text{Fe}_{1/2}\text{Nb}_{1/2})\text{O}_3$  recorded at 100 Oe field in three different cycles as labeled in the plot. The field is set to zero during the intermittent wait of cooling temperature  $T_w = 50, 15$  K for 3 h. The cooling and heating rate of measurement is 2 K/min. The pronounced steps in the cooling curve occurs at 15 K and no such step is seen above the spin glass freezing temperature (i.e., at 50 K).

both the temperatures. After the completion of the wait time, the field was reapplied and the measurement was resumed during further cooling. The  $M(T)$  curve so obtained is labeled as  $M_{\text{wait}}^{\text{FCC}}(T)$  and is shown with a plus (+) symbol in Fig. 9. After cooling the sample to the lowest temperature 2 K in this way, the magnetization [ $M_{\text{mem}}^{\text{FCW}}(T)$ ] measurement was carried out during heating cycle maintaining the same rate (i.e., 2 K/min) and the same field (i.e., 100 Oe). The results are shown with open (o) circles in Fig. 9. It is evident from the figure that the  $M_{\text{wait}}^{\text{FCC}}(T)$  curve shows a step at the wait temperature  $T_w = 15$  K below  $T_f$ . However, no such step is observed at the other wait temperature  $T_w = 50$  K greater than  $T_f \sim 25$  K. Further, all three curves merge above  $T_f$ . This protocol based on measurements done during both heating and cooling cycles further confirms that the sample remembers the measurement history. The observation memory and rejuvenation effect further rules out SPM blocking and confirms the existence of the glassy phase below  $T_f \sim 25$  K.

A slim hysteresis loop with nonzero remanence but without saturation opens up below  $T_f$  in conventional spin glasses as well as cluster spin glasses [60,61]. The  $M-H$  plot of CFN is linear at room temperature but shows a slim hysteresis loop with small remanent magnetization below  $T_f \sim 25$  K [see Fig. 10(a)]. The slim hysteresis loop does not saturate even at 7-T field at 5 K. The SG/CSG systems exhibit unidirectional exchange-bias effect [60,61]. To capture this effect,  $M-H$  hysteresis loops were recorded after cooling the sample from room temperature to 5 K, with proper thermal stabilization, under ZFC and 7-T FC conditions in two separate cycles. Proper precautions were taken to minimize the remanent field in the system that could have led to the observation of a minor hysteresis loop. The  $M-H$  loop of the field-cooled sample is found to be shifted in a direction opposite to the direction of the field with an exchange bias of  $H_{\text{ex}} \sim 118$  Oe [see Fig. 10(b)]. The  $M-H$  loop of the ZFC sample, on the

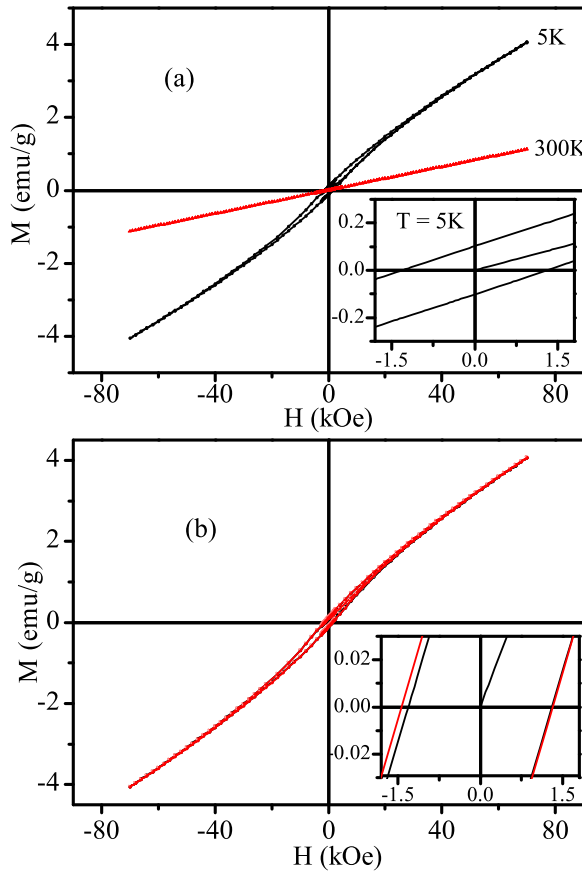


FIG. 10. (a) Magnetic-field dependence of isothermal magnetization of  $\text{Ca}(\text{Fe}_{1/2}\text{Nb}_{1/2})\text{O}_3$  sample at 5 and 300 K. Inset depicts the zoomed scale of  $M$ - $H$  curve in the low-field region at 5 K. (b) Depiction of magnetization as a function of magnetic field for  $\text{Ca}(\text{Fe}_{1/2}\text{Nb}_{1/2})\text{O}_3$  sample at 5 K in ZFC and 7-T FC conditions to measure the exchange-bias effect. Inset shows the enlarged scale of  $M$ - $H$  curve for low-field region.

other hand, does not show any unidirectional exchange bias. The appearance of such a unidirectional exchange bias in a direction opposite to the cooling field in the  $M$ - $H$  hysteresis loop of the FC sample confirms the existence of the glassy phase in CFN [60,61].

#### F. Direct evidence for the presence of spin clusters in CFN using neutron diffraction

The small dip in FCW  $M(T)$  plot just below the SG freezing temperature  $T_f$  in the ZFCW  $M(T)$  plot points towards the possibility of a CSG phase. Similarly, the large value of attempt time  $\tau_0$  ( $\sim 10^{-6}$  s), obtained from power-law and VF law fits to the temperature dependence of the spin-relaxation time, also suggests that the SG phase of CFN may be of CSG type [60,61]. Neutron-scattering technique can provide evidence not only for the presence of LRO AFM structure but also for short-range ordered (SRO) AFM clusters of spins in the CSG systems. The presence of SRO AFM spin clusters gives rise to diffuse scattering in the neutron-scattering patterns [46,74,94–98]. Accordingly, we carried out NPD measurements on powder samples of CFN to obtain direct evidence for the presence of AFM spin clusters.

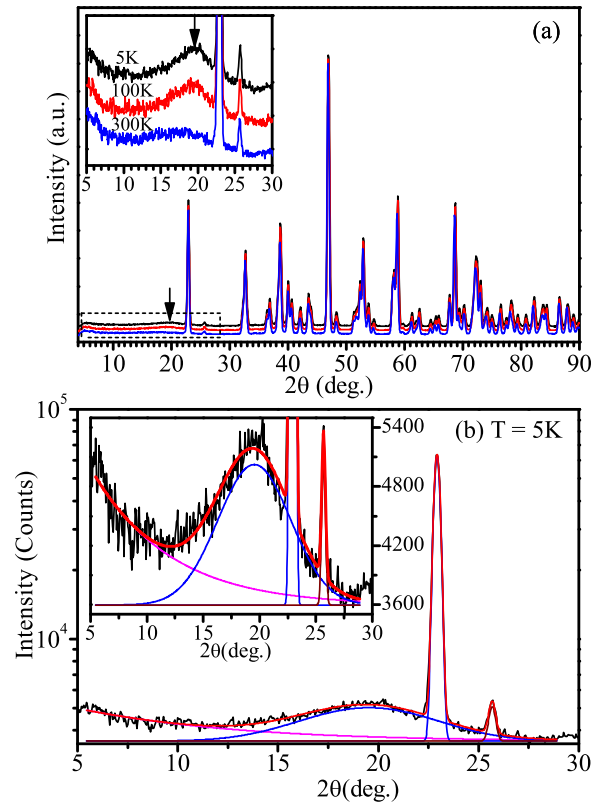


FIG. 11. Panel (a) depicts neutron powder-diffraction patterns of  $\text{Ca}(\text{Fe}_{1/2}\text{Nb}_{1/2})\text{O}_3$  collected at 300, 100, and 5 K. The patterns are shifted vertically for the purpose of presentation. Inset of (a) depicts the enlarged scale of broad diffuse magnetic scattering peak corresponding to short-range antiferromagnetic correlations. Panel (b) depicts the deconvolution of the NPD profile peaks at 5 K. Insets of panel (b) show enlarged scale of deconvoluted peaks at 5 K.

Figure 11(a) depicts the NPD patterns of CFN at three selected temperatures, 300, 100, and 5 K, over a limited  $2\theta$  range from  $5^\circ$  to  $90^\circ$ . For LRO AFM phase, one expects a sharp magnetic peak corresponding to the pseudocubic  $Q = 1/2 \ 1/2 \ 1/2$  position shown with an arrow in Fig. 11(a). It can be clearly seen from this figure that no sharp magnetic Bragg peak characteristic of LRO AFM phase is observed in the NPD patterns of CFN down to 5 K in marked contrast to PFN where such a peak has been observed [31]. Instead, a broad diffuse peak, whose peak intensity is about 4% of the strongest nuclear peak, centered at the expected position of AFM LRO peak, is clearly seen in Fig. 11(a). The observation of a broad diffuse peak provides direct evidence for the presence of SRO AFM spin clusters. A similar broad diffuse peak has been reported in geometrically frustrated pyrochlores [94,95], spin-chain compounds [96,97], and spinels [98] showing CSG freezing.

It is interesting to note from Fig. 11(a) that the broad peak due to the short-range AFM-correlated spin clusters is present even at room temperature, which is much higher than  $T_f \sim 25$  K. It is also evident from the figure that with decreasing temperature, the intensity of the broad diffuse peak increases. In order to determine the correlation length for AFM spin clusters from the magnetic diffuse scattering,

we deconvoluted the diffuse peak and the two neighboring stronger peaks using three Gaussians, and the results of the peak deconvolution are shown in Fig. 11(b). The deconvoluted diffuse magnetic peak centered at  $2\theta = 19.7^\circ$  at 5 K is shown in the inset of Fig. 11(b). It is possible to determine the correlation length ( $\xi$ ) from the full width at half maximum (FWHM) of the deconvoluted diffuse magnetic peak using the Scherrer formula  $\xi = 0.9\lambda/\beta \cos\theta$  ( $\text{\AA}$ ), after removing the instrumental broadening from the observed FWHM of the diffuse peak ( $\beta_{\text{obs}}$ ). We use the relationship  $\beta = \sqrt{\beta_{\text{obs}}^2 - \beta_{\text{inst}}^2}$ , where  $\beta$  is the intrinsic FWHM and  $\beta_{\text{inst}}$  is the FWHM of the instrumental resolution function. The correlation lengths for the SRO spin clusters obtained from the intrinsic FWHM are  $(22 \pm 1)$ ,  $(19 \pm 1)$ , and  $(14 \pm 2)$   $\text{\AA}$ , at 5, 100, and 300 K, respectively. Thus our neutron-scattering studies reveal that the size of the AFM-correlated spin clusters increases slightly on lowering the temperature, but the AFM correlations could not develop to long length scales presumably due to the frustrated nature of the superexchange interactions in CFN. Our neutron-scattering studies thus provide direct microscopic evidence for the presence of SRO AFM-correlated spin clusters of  $\sim 2$ -nm average size for CSG freezing in CFN.

#### IV. CONCLUSIONS

In summary, we investigated the low-temperature magnetic behavior of  $\text{Ca}(\text{Fe}_{1/2}\text{Nb}_{1/2})\text{O}_3$  using macroscopic and microscopic probes. Analysis of dc magnetization measurements reveals a spin glass phase with  $T_f \sim 25$  K with characteristic history-dependent irreversibility. Analysis of the ac susceptibility measurements reveals power-law/Vogel-Fulcher-type

critical spin dynamics with a time scale of  $\tau_0 \sim 10^{-6}$  s, which suggests the existence of a cluster spin glass phase in CFN below  $T_{\text{SG}} \sim 24$  K. The field dependence of the irreversibility temperature  $T_{\text{irr}}(H)$  and the peak temperature  $T_f(H)$  of the ZFCW  $M(T)$  falls on the de Almeida–Thouless line in a  $T_{\text{irr}}(H)/T_f(H)$  versus  $H^{2/3}$  plot. The zero-field SG freezing temperature  $T_f(0) = 25.2$  K, obtained from the extrapolation of  $T_f(H)$  versus  $H^{2/3}$  plot to  $H = 0$ , is in close agreement with the ergodicity-breaking temperature  $T_{\text{SG}} \sim 24$  K obtained from the analysis of the ac susceptibility  $\chi(\omega, T)$  data. The observation of slow relaxation of thermoremanent magnetization, memory and rejuvenation effects, and unidirectional exchange-bias effect below the SG transition temperature  $T_{\text{SG}} \sim 24$  K supports glassy phase. Neutron-diffraction study confirms the absence of any long-range AFM ordering but shows diffuse scattering due to the presence of short-range ordered AFM spin clusters with a correlation length  $\xi \sim 2$  nm involved in the CSG freezing.

#### ACKNOWLEDGMENTS

We thank Professor Chalapathi N. V. Rao, Department of Geology, Banaras Hindu University, Varanasi-221005 for the EPMA measurements. The authors also acknowledge the help of Mr. Girish Sahu in SEM and EDX analysis. Portions of this research were carried out at the light source PETRA III of DESY, a member of Helmholtz association (HGF). Financial support by the Department of Science and Technology (Government of India) provided within the framework of India@DESY collaboration, operated through Jawaharlal Nehru Centre for advanced Scientific Research (Jakkur), India is gratefully acknowledged.

- 
- [1] S. Vasala and M. Karppinen, *Prog. Solid State Chem.* **43**, 1 (2015).
- [2] H. J. Zhao, W. Ren, Y. Yang, J. Íñiguez, X. M. Chen, and L. Bellaiche, *Nat. Commun.* **10**, 535 (2014).
- [3] R. A. Cowley, S. N. Gvasaliya, S. G. Lushnikov, B. Roessli, and G. M. Rotaru, *Adv. Phys.* **60**, 229 (2011).
- [4] L. E. Cross, *Ferroelectrics* **151**, 305 (1994).
- [5] I.-K. Jeong, T. W. Darling, J. K. Lee, Th. Proffen, R. H. Heffner, J. S. Park, K. S. Hong, W. Dmowski, and T. Egami, *Phys. Rev. Lett.* **94**, 147602 (2005).
- [6] W. Ge, C. P. Devreugd, D. Phelan, Q. Zhang, M. Ahart, J. Li, H. Luo, L. A. Boatner, D. Viehland, and P. M. Gehring, *Phys. Rev. B* **88**, 174115 (2013).
- [7] S. Prosandeev and L. Bellaiche, *Phys. Rev. B* **94**, 80102(R) (2016).
- [8] S. Prosandeev, B. Xu, and L. Bellaiche, *Phys. Rev. B* **98**, 024105 (2018).
- [9] V. Sivasubramanian, V. Subramanian, and S. Kojima, *Phys. Rev. B* **93**, 054115 (2016).
- [10] N. Setter and L. E. Cross, *J. Mater. Sci.* **15**, 2478 (1980).
- [11] K.-I. Kobayashi, T. Kimura, H. Sawada, K. Terakura, and Y. Tokura, *Nature (London)* **395**, 677 (1998).
- [12] M. C. Viola, M. J. Martínez-Lope, J. A. Alonso, P. Velasco, J. L. Martínez, J. C. Pedregosa, R. E. Carbonio, and M. T. Fernández-Díaz, *Chem. Mater.* **14**, 812 (2002).
- [13] R. N. Mahato, K. Sethupathi, and V. Sankaranarayanan, *J. Appl. Phys.* **107**, 09D714 (2010).
- [14] O. Erten, O. N. Meetei, A. Mukherjee, M. Randeria, N. Trivedi, and P. Woodward, *Phys. Rev. Lett.* **107**, 257201 (2011).
- [15] M. Retuerto, M.-R. Li, P. W. Stephens, J. Sanchez-Benítez, X. Deng, G. Kotliar, M. C. Croft, A. Ignatov, D. Walker, and M. Greenblatt, *Chem. Mater.* **27**, 4450 (2015).
- [16] F. Estrada, E. J. Guzmán, O. Navarro, and M. Avignon, *Phys. Rev. B* **97**, 195155 (2018).
- [17] H. Kato, T. Okuda, Y. Okimoto, Y. Tomioka, K. Oikawa, T. Kamiyama, and Y. Tokura, *Phys. Rev. B* **65**, 144404 (2002).
- [18] Y. Krockenberger, K. Mogare, M. Reehuis, M. Tovar, M. Jansen, G. Vaitheeswaran, V. Kanchana, F. Bultmark, A. Delin, F. Wilhelm, A. Rogalev, A. Winkler, and L. Alff, *Phys. Rev. B* **75**, 020404(R) (2007).
- [19] V. N. Antonov, L. V. Bekenov, and A. Ernst, *Phys. Rev. B* **94**, 035122 (2016).
- [20] D. R. Harshman, W. J. Kossler, A. J. Greer, D. R. Noakes, C. E. Stronach, E. Koster, M. K. Wu, F. Z. Chien, J. P. Franck, I. Isaac, and J. D. Dow, *Phys. Rev. B* **67**, 054509 (2003).
- [21] M. H. K. Rubel, A. Miura, T. Takei, N. Kumada, M. M. Ali, M. Nagao, S. Watauchi, I. Tanaka, K. Oka, M. Azuma, E. Magome, C. Moriyoshi, Y. Kuroiwa, and A. K. M. A. Islam, *Angew. Chem. Int. Ed.* **53**, 3599 (2014).

- [22] F. Chu, N. Setter, and A. K. Tagantsev, *J. Appl. Phys.* **74**, 5129 (1993).
- [23] A. Levstik, V. Bobnar, C. Filipič, J. Holc, M. Kosec, R. Blinc, Z. Trontelj, and Z. Jagličič, *Appl. Phys. Lett.* **91**, 012905 (2007).
- [24] P. D. Battle, S. I. Evers, E. C. Hunter, and M. Westwood, *Inorg. Chem.* **52**, 6648 (2013).
- [25] B. Yan, A. K. Paul, S. Kanungo, M. Reehuis, A. Hoser, D. M. Többsen, W. Schnelle, R. C. Williams, T. Lancaster, F. Xiao, J. S. Möller, S. J. Blundell, W. Hayes, C. Felser, and M. Jansen, *Phys. Rev. Lett.* **112**, 147202 (2014).
- [26] D. Yang, R. J. Harrison, J. A. Schiemer, G. I. Lampronti, X. Liu, F. Zhang, H. Ding, Y. Liu, and M. A. Carpenter, *Phys. Rev. B* **93**, 024101 (2016).
- [27] M.-R. Li, P. W. Stephens, M. Croft, Z. Deng, W. Li, C. Jin, M. Retuerto, J. P. Hodge, C. E. Frank, M. Wu, D. Walker, and M. Greenblatt, *Chem. Mater.* **30**, 4508 (2018).
- [28] Y. K. Wakabayashi, Y. Krockenberger, N. Tsujimoto, T. Boykin, S. Tsuneyuki, Y. Taniyasu, and H. Yamamoto, *Nat. Commun.* **10**, 535 (2019).
- [29] K. Naveen, M. Reehuis, P. Adler, P. Pattison, A. Hoser, T. K. Mandal, U. Arjun, P. K. Mukharjee, R. Nath, C. Felser, and A. K. Paul, *Phys. Rev. B* **98**, 224423 (2018).
- [30] W. Kleemann, V. V. Shvartsman, P. Borisov, and A. Kania, *Phys. Rev. Lett.* **105**, 257202 (2010).
- [31] S. Chillal, M. Thede, F. J. Litterst, S. N. Gvasaliya, T. A. Shaplygina, S. G. Lushnikov, and A. Zheludev, *Phys. Rev. B* **87**, 220403(R) (2013).
- [32] M.-R. Li, P. W. Stephens, M. Retuerto, T. Sarkar, C. P. Grams, J. Hemberger, M. C. Croft, D. Walker, and M. Greenblatt, *J. Am. Chem. Soc.* **136**, 8508 (2014).
- [33] P. S. Wang, W. Ren, L. Bellaiche, and H. J. Xiang, *Phys. Rev. Lett.* **114**, 147204 (2015).
- [34] M.-R. Li, M. Croft, P. W. Stephens, M. Ye, D. Vanderbilt, M. Retuerto, Z. Deng, C. P. Grams, J. Hemberger, J. Hadermann, W.-M. Li, C.-Q. Jin, F. O. Saouma, J. I. Jang, H. Akamatsu, V. Gopalan, D. Walker, and M. Greenblatt, *Adv. Mater.* **27**, 2177 (2015).
- [35] J. Lohr, F. Pomiro, V. Pomjakushin, J. A. Alonso, R. E. Carbonio, and R. D. Sanchez, *Phys. Rev. B* **98**, 134405 (2018).
- [36] R. E. Cohen, *Nature (London)* **358**, 136 (1992).
- [37] G. A. Smolenskii, A. I. Agranovskaia, S. N. Popov, and V. A. Isupov, *Sov. Phys. Tech. Phys.* **3**, 1981 (1958).
- [38] G. A. Smolenskii, A. I. Agranovskaya, and V. A. Isupov, *Sov. Phys. Solid State* **1**, 149 (1959).
- [39] V. A. Bokov, I. I. Mylnikova, and G. A. Smolenskii, *Sov. Phys. JETP* **15**, 447 (1962).
- [40] S. P. Singh, A. K. Singh, D. Pandey, H. Sharma, and O. Prakash, *J. Mater. Res.* **18**, 2677 (2003).
- [41] R. Blinc, M. Kosec, J. Holc, Z. Trontelj, Z. Jaglicic, and N. Dalal, *Ferroelectrics* **349**, 16 (2007).
- [42] S. P. Singh, S. M. Yusuf, S. Yoon, S. Baik, N. Shin, and D. Pandey, *Acta Mater.* **58**, 5381 (2010).
- [43] N. Lampis, P. Sciau, and A. G. Lehmann, *J. Phys.: Condens. Matter* **11**, 3489 (1999).
- [44] S. P. Singh, D. Pandey, S. Yoon, S. Baik, and N. Shin, *Appl. Phys. Lett.* **90**, 242915 (2007).
- [45] S. A. Ivanov, R. Tellgren, H. Rundlof, N. W. Thomasand, and S. Ananta, *J. Phys.: Condens. Matter* **12**, 2393 (2000).
- [46] G. M. Rotaru, B. Roessli, A. Amato, S. N. Gvasaliya, C. Mudry, S. G. Lushnikov, and T. A. Shaplygina, *Phys. Rev. B* **79**, 184430 (2009).
- [47] M. A. de Vries, A. C. Mclaughlin, and J.-W. G. Bos, *Phys. Rev. Lett.* **104**, 177202 (2010).
- [48] A. K. Azad, J. M. Wikberg, S.-G. Eriksson, A. Khan, P. Svedlindh, and J. T. S. Irvine, *Phys. Rev. B* **77**, 064418 (2008).
- [49] C. R. Wiebe, J. E. Greedan, P. P. Kyriakou, G. M. Luke, J. S. Gardner, A. Fukaya, I. M. Gat-Malureanu, P. L. Russo, A. T. Savici, and Y. J. Uemura, *Phys. Rev. B* **68**, 134410 (2003).
- [50] R. Pradheesh, H. S. Nair, G. R. HariPriya, A. Senyshyn, T. Chatterji, V. Sankaranarayanan, and K. Sethupathi, *J. Phys.: Condens. Matter.* **29**, 095801 (2017).
- [51] J. K. Murthy and A. Venimadhav, *J. Appl. Phys.* **113**, 163906 (2013).
- [52] P. D. Battle, T. C. Gibb, C. W. Jones, and F. Studer, *J. Solid State Chem.* **78**, 281 (1989).
- [53] A. B. Harris, *J. Phys. C: Solid State Phys.* **7**, 1671 (1974).
- [54] I. P. Raevski, S. P. Kubrin, S. I. Raevskaya, V. V. Titov, D. A. Sarychev, M. A. Malitskaya, I. N. Zakharchenko, and S. A. Prosandeev, *Phys. Rev. B* **80**, 024108 (2009).
- [55] R. Rodríguez, A. Fernández, A. Isalgué, J. Rodríguez, A. Labrata, J. Tejada, and X. Obradors, *J. Phys. C: Solid State Phys.* **18**, L401 (1985).
- [56] P. D. Battle, T. C. Gibb, A. J. Herod, S.-H. Kim, and P. H. Munns, *J. Mater. Chem.* **5**, 865 (1995).
- [57] K. Tezuka, K. Henmi, Y. Hinatsu, and N. M. Masaki, *J. Solid State Chem.* **154**, 591 (2000).
- [58] M. Maryško, V. V. Laguta, I. P. Raevski, R. O. Kuzian, N. M. Olekhnovich, A. V. Pushkarev, Y. V. Radyush, S. I. Raevskaya, V. V. Titov, and S. P. Kubrin, *AIP Adv.* **7**, 056409 (2017).
- [59] S. Bedanta and W. Kleemann, *J. Phys. D: Appl. Phys.* **42**, 013001 (2009).
- [60] J. A. Mydosh, *Spin Glass: An Experimental Introduction* (Taylor and Francis, London, 1993).
- [61] K. Binder and A. P. Young, *Rev. Mod. Phys.* **58**, 801 (1986).
- [62] J. Rodriguez-Carvajal, FULLPROF, a Rietveld and pattern matching and analysis program, Version 2018, Laboratoire Leon Brillouin, CEA-CNRS, France; <http://www.ill.eu/sites/fullprof/>
- [63] Y. Y. Liu, M. X. Chen, X. Q. Liu, and L. Li, *Appl. Phys. Lett.* **90**, 262904 (2007).
- [64] I. O. Troyanchuk, N. V. Tereshko, and M. V. Bushinskiĭ, *Phys. Solid State* **51**, 785 (2009).
- [65] A. M. Glazer, *Acta Crystallogr. Sect. B: Struct. Crystallogr. Cryst. Chem.* **28**, 3384 (1972).
- [66] P. W. Barnes, M. W. Lufaso, and P. M. Woodward, *Acta Crystallogr., Sect. B: Struct. Sci.* **62**, 384 (2006).
- [67] M. W. Lufaso, P. M. Woodward, and J. Goldberger, *J. Solid State Chem.* **177**, 1651 (2004).
- [68] See Supplemental Material at <http://link.aps.org/supplemental/10.1103/PhysRevB.99.214425> for details of room temperature crystal structure of  $\text{Ca}(\text{Fe}_{1/2}\text{Nb}_{1/2})\text{O}_3$  using monoclinic space group ( $\text{P}2_1/n$ ).
- [69] S. Chillal, S. N. Gvasaliya, A. Zheludev, D. Schroeter, M. Kraken, F. J. Litterst, T. A. Shaplygina, and S. G. Lushnikov, *Phys. Rev. B* **89**, 174418 (2014).
- [70] V. V. Laguta, M. D. Glinchuk, M. Maryško, R. O. Kuzian, S. A. Prosandeev, S. I. Raevskaya, V. G. Smotrakov, V. V. Eremkin, and I. P. Raevski, *Phys. Rev. B* **87**, 064403 (2013).

- [71] L. Chen, A. A. Bokov, W. Zhu, H. Wu, J. Zhuang, N. Zhang, H. N. Tailor, W. Ren, and Z.-G. Ye, *Sci. Rep.* **6**, 22327 (2016).
- [72] N. Marcano, P. A. Algarabel, L. Fernández Barquín, J. P. Araujo, A. M. Pereira, J. H. Belo, C. Magén, L. Morellón, and M. R. Ibarra, *Phys. Rev. B* **99**, 054419 (2019).
- [73] K. Gunnarsson, P. Svedlindh, P. Nordblad, L. Lundgren, H. Aruga, and A. Ito, *Phys. Rev. Lett.* **61**, 754 (1988).
- [74] V. K. Anand, L. Opherden, J. Xu, D. T. Adroja, A. D. Hillier, P. K. Biswas, T. Herrmannsdörfer, M. Uhlarz, J. Hornung, J. Wosnitza, E. Canévet, and B. Lake, *Phys. Rev. B* **97**, 094402 (2018).
- [75] N. Hanasaki, K. Watanabe, T. Ohtsuka, I. Kézsmárki, S. Iguchi, S. Miyasaka, and Y. Tokura, *Phys. Rev. Lett.* **99**, 086401 (2007).
- [76] L. J. Vera Stimpson, J. M. Powell, G. B. G. Stenning, M. Jura, and D. C. Arnold, *Phys. Rev. B* **98**, 174429 (2018).
- [77] J. L. Tholence, *Solid State Commun.* **35**, 113 (1980).
- [78] G. Parisi, *Phys. Rev. Lett.* **43**, 1754 (1979).
- [79] J. R. L. de Almeida and D. J. Thouless, *J. Phys. A: Math. Gen.* **11**, 983 (1978).
- [80] M. Gabay and G. Toulouse, *Phys. Rev. Lett.* **47**, 201 (1981).
- [81] D. M. Cragg, D. Sherrington, and M. Gabay, *Phys. Rev. Lett.* **49**, 158 (1982).
- [82] D. M. Cragg and D. Sherrington, *Phys. Rev. Lett.* **49**, 1190 (1982).
- [83] P. Bag, P. R. Baral, and R. Nath, *Phys. Rev. B* **98**, 144436 (2018).
- [84] P. M. Shand, T. Rash, M. Streicher, T. E. Kidd, K. R. Boyle, and L. H. Strauss, *Phys. Rev. B* **82**, 214413 (2010).
- [85] B. Martínez, X. Obradors, Ll. Balcells, A. Rouanet, and C. Monty, *Phys. Rev. Lett.* **80**, 181 (1998).
- [86] M. D. Mukadam, S. M. Yusuf, P. Sharma, S. K. Kulshreshtha, and G. K. Dey, *Phys. Rev. B* **72**, 174408 (2005).
- [87] S. Ghara, B.-G. Jeon, K. Yoo, K. H. Kim, and A. Sundaresan, *Phys. Rev. B* **90**, 024413 (2014).
- [88] X. K. Zhang, J. J. Yuan, Y. M. Xie, Y. Yu, F. G. Kuang, H. J. Yu, X. R. Zhu, and H. Shen, *Phys. Rev. B* **97**, 104405 (2018).
- [89] A. Kumar, S. D. Kaushik, V. Siruguri, and D. Pandey, *Phys. Rev. B* **97**, 104402 (2018).
- [90] R. G. Palmer, D. L. Stein, E. Abrahams, and P. W. Anderson, *Phys. Rev. Lett.* **53**, 958 (1984).
- [91] K. Jonason, E. Vincent, J. Hammann, J. P. Bouchaud, and P. Nordblad, *Phys. Rev. Lett.* **81**, 3243 (1998).
- [92] Y. Sun, M. B. Salamon, K. Garnier, and R. S. Averback, *Phys. Rev. Lett.* **91**, 167206 (2003).
- [93] A. J. Bray and M. A. Moore, *Phys. Rev. Lett.* **58**, 57 (1987).
- [94] E. Granado, J. W. Lynn, R. F. Jardim, and M. S. Torikachvili, *Phys. Rev. Lett.* **110**, 017202 (2013).
- [95] Z. Fu, Y. Zheng, Y. Xiao, S. Bedanta, A. Senyshyn, G. G. Simeoni, Y. Su, U. Rücker, P. Kögerler, and T. Brückel, *Phys. Rev. B* **87**, 214406 (2013).
- [96] A. K. Bera, S. M. Yusuf, A. Kumar, M. Majumder, K. Ghoshray, and L. Keller, *Phys. Rev. B* **93**, 184409 (2016).
- [97] A. K. Bera, S. M. Yusuf, A. Kumar, and C. Ritter, *Phys. Rev. B* **95**, 094424 (2017).
- [98] K. Tomiyasu, J. Fukunaga, and H. Suzuki, *Phys. Rev. B* **70**, 214434 (2004).